AGU PUBLICATIONS

Geophysical Research Letters

RESEARCH LETTER
10.1002/2017GL073156

Special Section:
Early Results: Juno at Jupiter

Variability of Jupiter's IR H_3^+ aurorae during Juno approach

L. Moore[1], J. O'Donoghue[2], H. Melin[3], T. Stallard[3], C. Tao[4], B. Zieger[1], J. Clarke[1], M. F. Vogt[1], T. Bhakyapaibul[1], M. Opher[1], G. Tóth[5], J. E. P. Connerney[2], S. Levin[6], and S. Bolton[7]

[1]Center for Space Physics, Boston University, Boston, Massachusetts, USA, [2]NASA Goddard Space Flight Center, Greenbelt, Maryland, USA, [3]Department of Physics and Astronomy, University of Leicester, Leicester, UK, [4]National Institute of Information and Communications Technology, Tokyo, Japan, [5]Center for Space Environment Modeling, University of Michigan, Ann Arbor, Michigan, USA, [6]Jet Propulsion Laboratory, Pasadena, California, USA, [7]Southwest Research Institute, San Antonio, Texas, USA

Key Points:
- For the first time, Jupiter's auroral temperatures are mapped, while the upstream solar wind magnetic field is measured in situ
- Maps of northern and southern H_3^+ aurorae show significant variability in four observations spaced across 11 days
- Auroral H_3^+ intensifications are found to be dominated by density enhancements rather than temperature increases

Correspondence to:
L. Moore,
moore@bu.edu

Citation:
Moore, L., et al. (2017), Variability of Jupiter's IR H_3^+ aurorae during Juno approach, *Geophys. Res. Lett.*, *44*, 4513–4522, doi:10.1002/2017GL073156.

Received 19 FEB 2017
Accepted 2 MAY 2017
Published online 25 MAY 2017

Abstract We present ground-based observations of Jupiter's H_3^+ aurorae over four nights in April 2016 while the Juno spacecraft was monitoring the upstream interplanetary magnetic field. High-precision maps of auroral H_3^+ densities, temperatures, and radiances reveal significant variabilities in those parameters, with regions of enhanced density and emission accompanied by reduced temperature. Juno magnetometer data, combined with solar wind propagation models, suggest that a shock may have impacted Jupiter in the days preceding the observation interval but that the solar wind was quiescent thereafter. Auroral H_3^+ temperatures reveal a downward temporal trend, consistent with a slowly cooling upper atmosphere, such as might follow a period of shock recovery. The brightest H_3^+ emissions are from the end of the period, 23 April. A lack of definitive signatures in the upstream interplanetary magnetic field lends supporting evidence to the possibility that this brightening event may have been driven by internal magnetospheric processes.

1. Introduction

Planetary aurorae are a visible manifestation of a coupling process between an atmosphere and the nearby space environment. At Earth, this coupling process extends ultimately to the Sun, as auroral enhancements are strongly correlated with changes in upstream solar wind conditions that disturb the terrestrial magnetosphere. Both a southward turning of the interplanetary magnetic field (IMF) and a solar wind dynamic pressure pulse can drive global auroral brightening events [e.g., *Elphinstone et al.*, 1996; *Chua et al.*, 2001].

Jupiter's magnetosphere, in contrast to Earth's, is filled with high-density plasma as explained in *Thomas et al.* [2004], and its main auroral emissions can be traced back to the middle magnetospheric region far from the solar wind boundary [*Hill*, 2004]. The solar wind's influence on Jupiter's aurorae, while still present, has proven more difficult to clearly isolate from internal processes, largely due to two factors: a lack of upstream solar wind measurements close to Jupiter and an uncertainty regarding the time scales for propagation of solar wind-induced shocks through Jupiter's large, dynamic magnetosphere.

Jupiter's aurorae emit in wavelengths from the radio to the X-ray, and auroral activity across each wave band is modulated by the solar wind to some degree. Auroral brightenings in the ultraviolet (UV) have been found to correlate with multiple sources: interplanetary shock arrivals associated with magnetospheric compression events [e.g., *Nichols et al.*, 2007; *Clarke et al.*, 2009], which also modify the observed auroral morphology [*Nichols et al.*, 2009]; internally driven aurorae associated with mass loading and related plasma circulation [*Bonfond et al.*, 2012; *Kimura et al.*, 2015]; and a third source causing UV aurorae to vary independently of both solar wind pressure and Io mass loading [*Clarke et al.*, 2009; *Badman et al.*, 2016].

Protonated molecular hydrogen, or H_3^+, is a major ion in any H_2 atmosphere, and its emissions dominate the near-IR giant planet aurorae. As H_3^+ is thought to be in quasi-local thermodynamic equilibrium with the surrounding neutral atmosphere [e.g., *Miller et al.*, 2000; *Melin et al.*, 2005; *Tao et al.*, 2011], a measurement of the H_3^+ temperature can be used as a proxy for the thermospheric temperature, thereby providing insight into the energetics of Jupiter's upper atmosphere. Auroral H_3^+ emissions are distinct in that, rather than representing an instantaneous view of the particle precipitation process (e.g., as in the UV), they depend on both the density and the temperature of the emitting ions, and these parameters can vary over longer time scales and broader spatial scales. The first indication that Jupiter's IR aurorae are modulated by

conditions in the solar wind was based on observations of H_3^+ emissions by NASA's Infrared Telescope Facility [*Baron et al.*, 1996], but these were unable to determine whether those intensity variations were associated primarily with H_3^+ density or temperature fluctuations.

The approach of the Juno spacecraft [*Bolton et al.*, 2010] in 2016 offered new opportunities to study the solar wind influence on Jupiter's aurorae and magnetosphere and to test the accuracy of solar wind propagation models. In this paper, we report on new observations of Jupiter's H_3^+ aurorae spread across 11 days in April 2016 when Juno was monitoring the upstream IMF.

2. Data

2.1. Ground-Based IR Observations

High-resolution (R ~ 25,000) spectroscopic data of Jupiter spanning 3.26–4 μm were obtained over four nights in April 2016 using the Near InfraRed Spectrograph (NIRSPEC) [*Mclean et al.*, 1998] on the 10 m Keck II telescope. These wavelengths encompass a myriad of rotational-vibrational H_3^+ transitions, primarily in the ν_2 fundamental band. Emissions from hydrocarbons in Jupiter's lower atmosphere are also present in this spectral window, though near 3.4 μm H_3^+ appears as a bright emission against a dark background as methane absorbs the majority of emission from below the homopause. Each night of observations—14, 17, 20, and 23 April—spanned approximately 04:00 to 10:00 UTC. Due to Jupiter's ~ 10 h day, each night also obtained just over 180° coverage in longitude, as the spectral slit was predominantly oriented north-south at local solar noon while Jupiter rotated. The combined data coverage from all four nights is illustrated in Figure 1a. Jupiter's equatorial angular diameter was approximately 42″ over the course of the observing campaign, and so in order to capture both Jupiter's northern and southern aurorae using NIRSPEC's 0.432″ × 24″ slit the telescope was continuously "nodded" between positions in Jupiter's north and south before moving to the sky (to enable sky background subtractions). The raw data product from these observations is therefore a series of spectral images, such as shown in Figure 1b.

In order to determine the position of the spectral slit, simultaneous slit-cam (SCAM) images of Jupiter were obtained using NIRSPEC's KL filter (2.16–4.19 μm). These SCAM images were then temporally matched with each spectrum, and the position of Jupiter's limb was determined. Uncertainty in limb fitting is estimated to be $<3°$ in longitude and $<1°$ in latitude. By projecting an oblate spheroid onto the plane of the image based on the known Earth-Jupiter geometry, and by extracting each of the seeing-widened pixel positions along the slit, we then obtained the spatial coverage for each spectrum in terms of Jupiter system III central meridian longitude (CML) and planetocentric latitude (lat_{pc}). To increase the signal-to-noise ratio, the spectra were then binned in CMLxlat_{pc} pixels of 4° × 2°. An example of the NIRSPEC slit, as mapped to Jupiter, is given by the cyan contour in Figure 1a, which spans a wider range of longitude at higher latitudes. Therefore, each individual spectrum is mapped across multiple 4° × 2° pixels, while the spectrum contained within each pixel represents the normalized sum of multiple overlapping spectra.

Three color-coded regions are identified by dashed boxes in Figure 1a. These regions represent the most active portions of the northern or southern aurorae for which there are multiple nights of coverage, and auroral variability in these regions can therefore be compared with solar wind variations.

Five spectral orders covering 3.26–4 μm spanned the NIRSPEC detector. Wavelength calibration, order extraction, and straightening were performed using the REDSPEC package (http://www2.keck.hawaii.edu/inst/nirspec/redspec.html). Subtraction of nearby interpolated sky frames—combined with flat-field, dark current, and line-of-sight (cosine of the emission angle) corrections—then yielded cleaned spectra in counts/s. Finally, absolute flux was obtained using spectra obtained for the photometric-standard A0V star HR2250.

These calibrated spectral orders covered two well-studied regions of ionospheric H_3^+ emission, the Q-branch (3.946–4.006 μm) and the R-branch (3.410–3.462 μm). Using established Gaussian line-fitting measurement techniques [e.g., *Stallard et al.*, 2002], a combination of the observed H_3^+ R- and Q-branch lines is compared with modeled H_3^+ spectra in order to derive vibrational temperature, column density, and total radiance [*Melin et al.*, 2014]. Measured line ratios yield temperature, which allows direct determination of density when combined with the observed intensity, and finally, the total radiance is calculated by integrating the resulting model spectrum over all wavelengths [*O'Donoghue et al.*, 2016]. This fitting procedure makes use of a complete spectroscopic H_3^+ line list [*Neale et al.*, 1996] and the most recent H_3^+ partition function

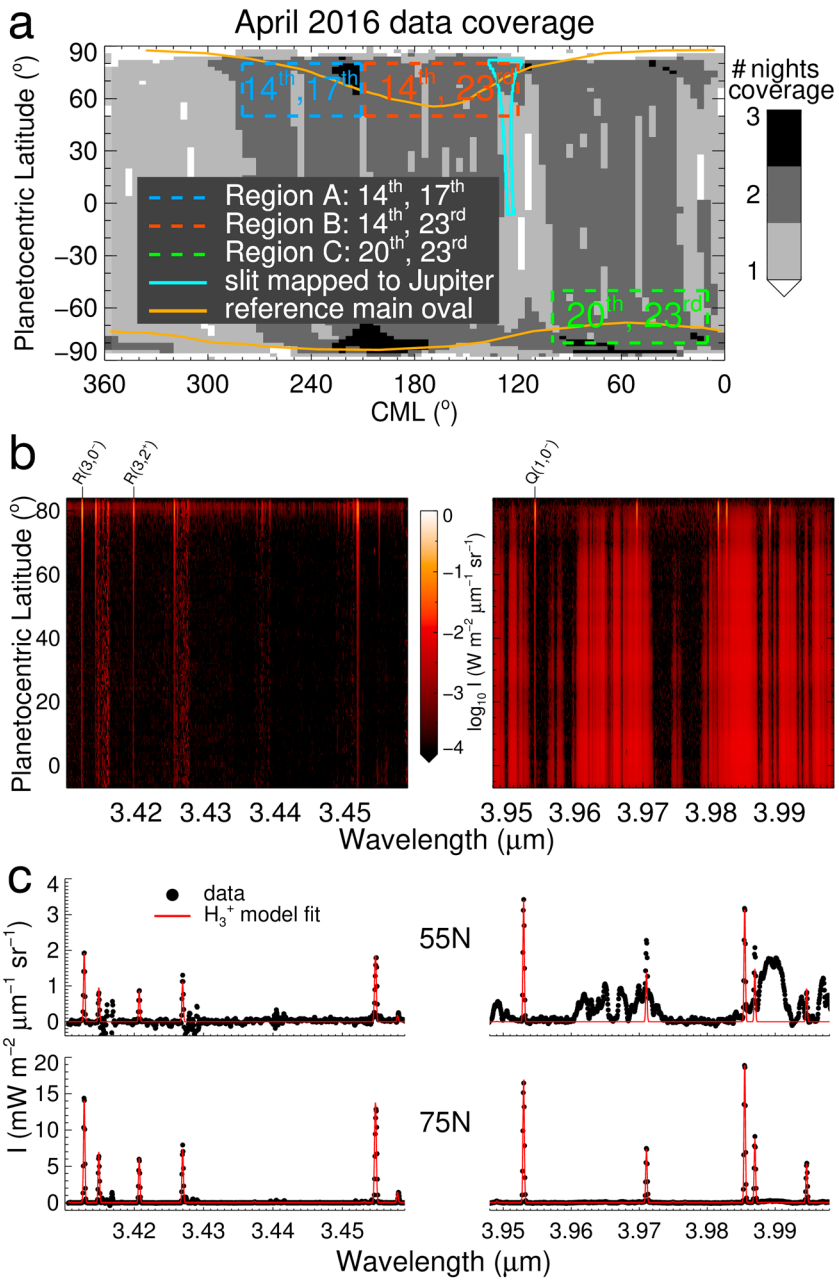

Figure 1. Data coverage and sample spectra. (a) Data coverage for the April 2016 Keck campaign, with the number of nights with viable H_3^+ spectra for each longitude/latitude element indicated by gray shading. The seeing-widened slit, mapped to Jupiter, is given by the cyan contour. The orange curves mark the reference main auroral oval positions [*Connerney et al.*, 1998]. The colored, dashed lines outline active auroral regions for which there were multiple nights of coverage over the campaign, with the corresponding dates indicated. (b) Typical spectral images of Jupiter obtained by Keck/NIRSPEC near 3.4 μm and 4 μm. A few prominent H_3^+ lines, well separated from other telluric and Jupiter emissions, are identified. (c) Observed spectra (black) and H_3^+ model fits (red) from 55°N and 75°N planetocentric latitude, 122 CML.

coefficients [*Miller et al.*, 2010]. At auroral latitudes, H_3^+ rotational-vibrational emissions completely dominate the observed spectrum, and so the entire Q-branch on order 1 of the detector is used to derive a model fit (3.946–4.006 μm). At lower latitudes (equatorward of ~68°N and ~76°S), additional planetary emissions from the underlying atmosphere become detectable, and so two H_3^+ lines isolated from telluric and other Jovian emissions are used, $R(3,2^+)$ at 3.4207 μm and $Q(1,0^-)$ at 3.953 μm. Derived temperature and density uncertainties in both cases are on the order of a few percent, owing to the quality of the data and the

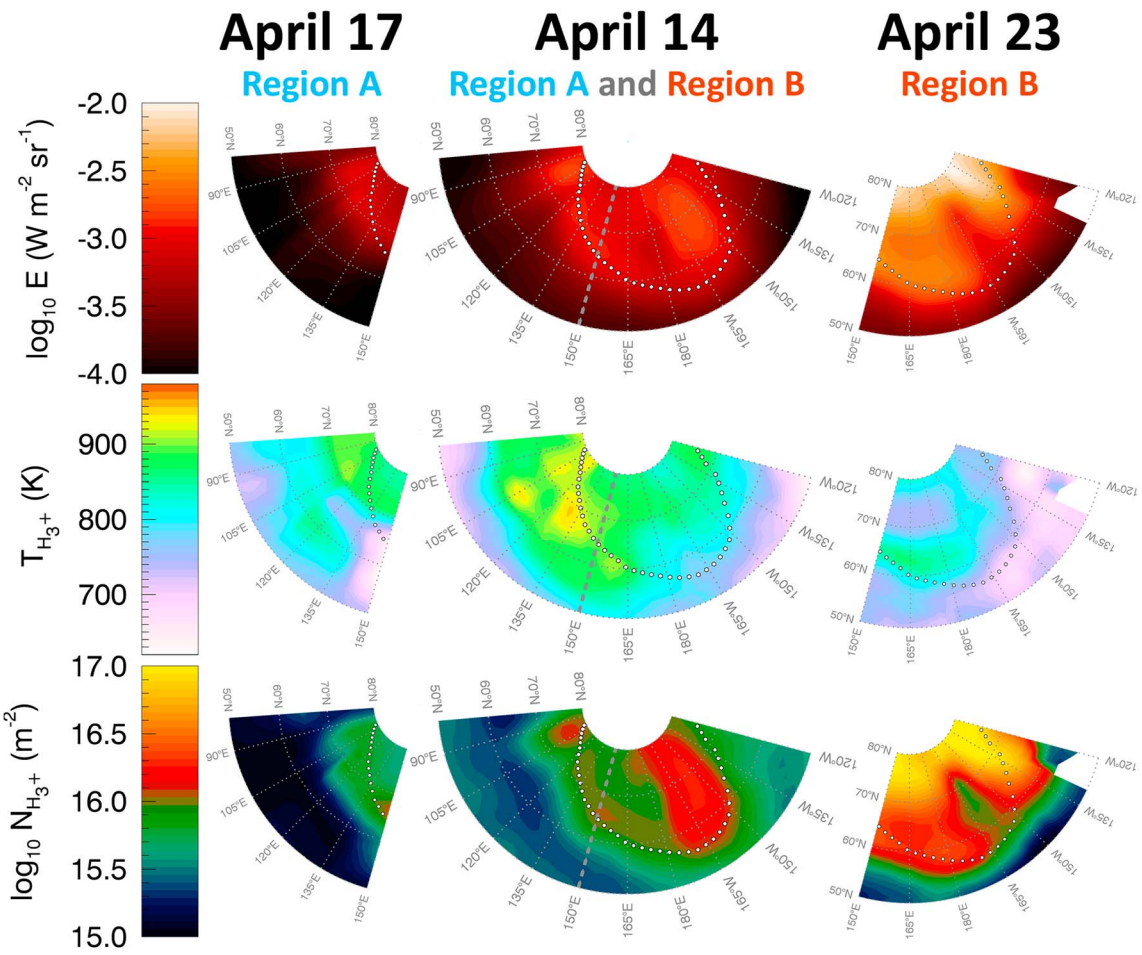

Figure 2. Derived ionospheric H_3^+ parameters in Regions A and B: Jupiter's northern aurora. The contours of (top) radiance, (middle row) column averaged temperature, and (bottom) column density for observations on (left) 17 April, (middle column) 14 April, and (right) 23 April. The gray dashed line in the 14 April plots marks the separation between Regions A and B. The white dots mark the statistical location of the main auroral oval [*Connerney et al.*, 1998]. The degree markings indicate northern planetocentric latitude and CML. The irregular white regions indicate data gaps.

bright auroral emissions. Representative observed spectra, along with corresponding H_3^+ model fits, are shown in Figure 1c. The chosen latitudes, 55°N and 75°N, represent the two different regimes for fitting the observed H_3^+ spectrum described above and demonstrate that both approaches are able to reproduce the majority of observed H_3^+ lines (the discrepancy near 3.427 μm is due to telluric contamination).

2.2. Juno Solar Wind Measurements and Corresponding Modeling

The Juno spacecraft has a full suite of particle and field instruments [*Bagenal et al.*, 2014]; however, during the period of study the only operating instrument relevant to sampling the upstream solar wind conditions was the magnetometer (MAG) [*Connerney et al.*, 2017]. Therefore, in order to complement the in situ Juno magnetic field measurements, we also show results from two solar wind propagation models. These models offer predictions for a number of additional solar wind parameters. Where they are able to make accurate magnetic field predictions, based on comparisons with Juno, we can feel confident in drawing upon the additional insight they provide.

Both solar wind propagation models used in this study are magnetohydrodynamic (MHD) codes situated in the solar equatorial plane, and both set their inner boundary using near-Earth solar wind observations. Uncertainties in propagated parameters for both models increase with Earth-Sun-Jupiter angle. Here this angle is between 17° (on 14 April) and 24° (on 24 April), so that solar wind extrapolations from this period should have a relatively high accuracy for both models (i.e., better than 20 h for shock arrival predictions and uncertainties <38% in maximum pressure values) [*Tao et al.*, 2005; *Kita et al.*, 2016].

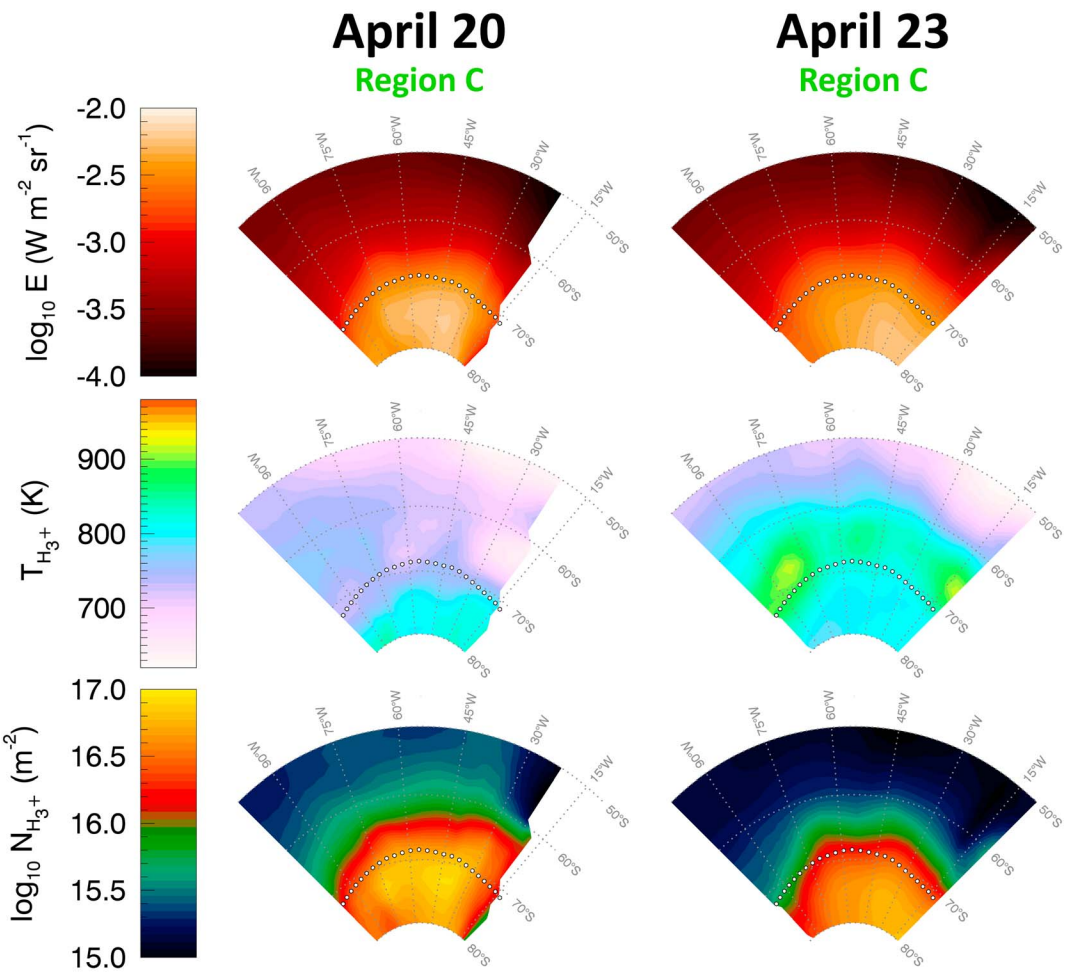

Figure 3. Derived ionospheric H_3^+ parameters in Region C: Jupiter's southern aurora, following the format of Figure 2.

The first model, the Space Weather Modeling Framework model of the Outer Heliosphere, hereafter referred to as SWMF-OH [*Zieger et al.*, 2015], is a 2-D MHD model based on the Space Weather Modeling Framework [*Tóth et al.*, 2012; *Opher et al.*, 2006, 2009]. The second solar wind propagation model is a 1-D MHD model developed by *Tao et al.* [2005], hereafter referred to as Tao-MHD.

3. Results and Discussion

3.1. H_3^+ Auroral Variability

Derived H_3^+ parameters, based on fits to the ground-based spectra, are given in Figure 2 for Regions A and B of the northern aurora and in Figure 3 for Region C of the southern aurora. It should be noted that (a) each image is constructed from a series of 1 min integrations (i.e., longitudinal slices) of auroral H_3^+ parameters obtained over the course of ~116 (Region A) or ~150 (Regions B and C) minutes and that (b) these images provide no local time information, as the spectral slit was aligned north-south along Jupiter's central meridian. Despite these differences from "typical" auroral images, the maps in Figures 2 and 3 still evince Jupiter's main auroral features. In particular, the majority of the observed H_3^+ emission is clearly on or poleward of the statistical location of the main auroral oval [*Connerney et al.*, 1998], illustrated by white dots.

In Figure 2, the radiance, density, and temperature of Jupiter's northern auroral region are shown for 3 days. There is significant variation in all three H_3^+ parameters, with particularly strong poleward enhancements in radiance and density evident on 23 April. For example, within Region B between 14 and 23 April, the mean H_3^+ column density increased by a factor of 3.65 (from 1.03×10^{16} m^{-2} to 3.75×10^{16} m^{-2}), the mean

radiance increased by a factor of 2.8 (from 0.925 mW m^{-2} sr^{-1} to 2.59 mW m^{-2} sr^{-2}), and the mean temperature decreased by 60 K (from 835 K to 775 K). Such an anticorrelation between density and temperature has been seen before and has been demonstrated to be due to a physical anticorrelation within Jupiter's atmosphere rather than any artifact of the H_3^+ emission fitting [*Melin et al.*, 2014].

One response of Jupiter's upper atmosphere to an enhanced flux of energetic particle precipitation is an increase in H_3^+ density, as the primary product of impact ionization at Jupiter is H_2^+, which reacts rapidly with H_2 to produce H_3^+ [*Grodent et al.*, 2001; *Galand et al.*, 2011; *Tao et al.*, 2011]. This increase in H_3^+ density is accompanied by a corresponding linear increase in emission. Temperature variations, on the other hand, are more complicated. If the H_3^+ ions are thermalized to the neutral atmosphere, as expected, then their temperature is representative of the thermospheric temperature structure, which itself varies in accordance with aurorally driven currents (among other factors) [*Majeed et al.*, 2009; *Smith and Aylward*, 2009; *Müller-Wodarg et al.*, 2012; *Yates et al.*, 2014].

As an optically thin emission, the derived H_3^+ temperature is a column-averaged value, a convolution of the altitude profiles of temperature and density. Thermospheric temperature increases with altitude [*Seiff*, 1997; *Majeed et al.*, 2009], while an increase in the energy of the precipitating particles generates more ionization at lower altitudes [*Millward et al.*, 2002; *Galand et al.*, 2011; *Tao et al.*, 2011; *Gérard et al.*, 2014]. Consequently, precipitation by particles with more energy would lead to a lower altitude peak for auroral H_3^+, and the derived temperature would therefore be representative of the lower altitude, lower temperature thermosphere.

Based on the preceding discussion, the transition from a "typical" H_3^+ auroral structure in the northern hemisphere on 14 April (Figure 2, Region B) to one enhanced in radiance and density, yet significantly reduced in temperature, is consistent with increases in both the mean energy and energy flux of precipitating particles. Jupiter's southern H_3^+ auroral region exhibits a similar behavior, as shown in Figure 3: between 20 and 23 April the radiance and density peaks shifted equatorward, and this shift appears to be correlated with a reduction in temperature surrounding the statistical main auroral oval location. In other words, in the presence of enhanced aurorae, based on the total H_3^+ radiance, we observe in both hemispheres a corresponding enhancement in column density and a reduction in temperature that may be representative of a preferential sampling of low-altitude H_3^+ driven by a larger flux of more energetic particle precipitation.

The above explanation implicitly assumes that temperatures in Jupiter's auroral thermosphere have not changed significantly over the period of observations. An alternative explanation to the observed H_3^+ variations is therefore one in which the changes in observed temperature are driven by auroral heating (cooling) events rather than by H_3^+ density profiles situated at higher (lower) altitudes. Of course, some combination of both explanations (and possibly others) is likely a better approximation of the truth, but we lack the observational constraints to be that precise and so instead focus on two broad extremes.

If we assume that the mean auroral temperature structure across each region from Figures 2 and 3 represents real upper atmospheric temperature changes, then we have two general observational constraints to explain. First, the largest mean temperatures are from 14 April (867 K over Region A and 834 K over Region B). Second, there is a general cooling trend in mean temperature with time, from 851 K on 14 April (across the combined Regions A and B), to 824 K on 17 April, to 820 K on 20 April, and to 767 K in the north and 775 K in the south on 23 April. We look to the corresponding solar wind observations and model results in order find self-consistent explanations of these constraints.

3.2. Correlations Between Jupiter's Aurorae and the Solar Wind

A comparison of auroral H_3^+ parameters to Juno in situ measurements and solar wind propagation model predictions is given in Figure 4. In the top half of the figure, each region identified in Figure 1a is represented by different colored symbols. As a rough method of representing auroral variability, the symbols simply give the arithmetic mean for each of the three regions shown in Figures 2 and 3. Data gaps present for one night of observation, but not for another covering the same region, are omitted from both regions when calculating the means to ensure a like-for-like comparison. The bottom half of the figure shows the corresponding upstream solar wind parameters, as measured in situ by Juno (magnetic field, black lines), and at Jupiter as predicted by the solar wind propagation models Tao-MHD (red dotted lines) and

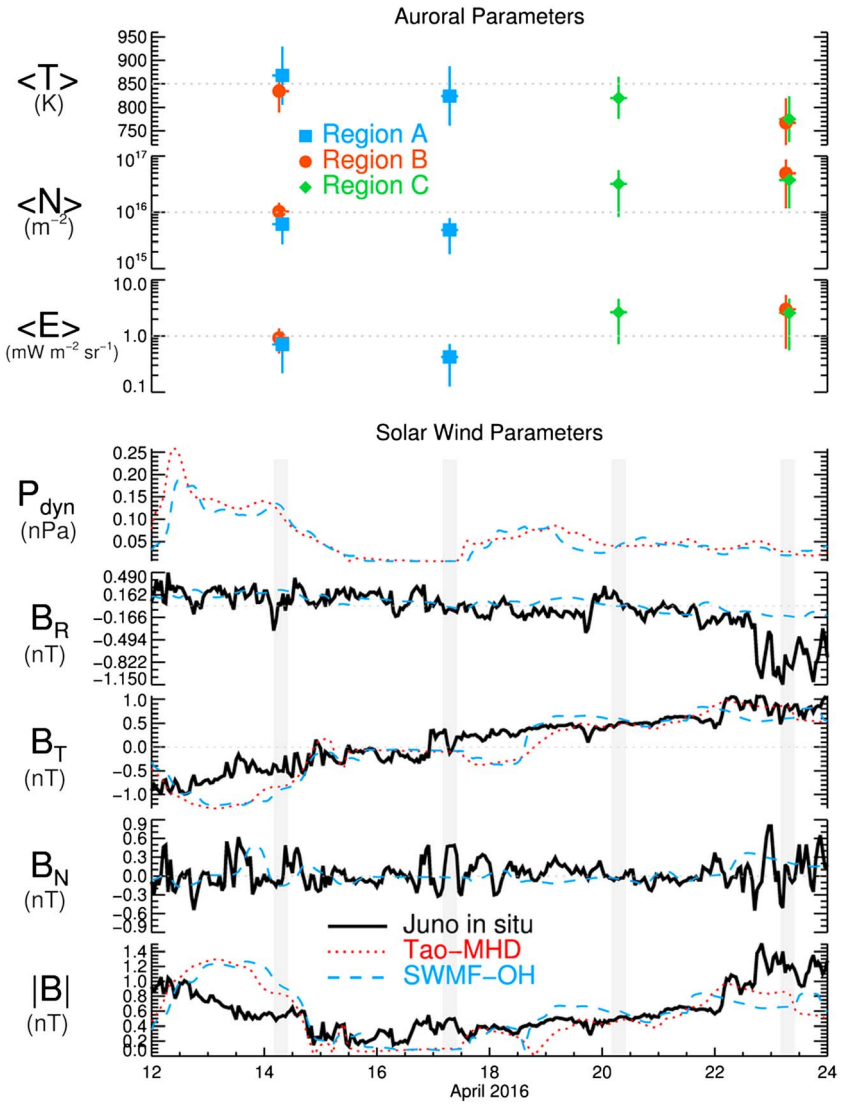

Figure 4. Comparison between variations in H_3^+ aurorae and the solar wind. (top half) Mean values for H_3^+ temperature, density, and radiance. The vertical error bars are the standard deviation of the mean, while the horizontal error bars indicate the timeframe over which the data were collected. (bottom half) Solar wind parameters measured in situ by Juno (IMF only, black lines) and predicted at Jupiter by two solar wind propagation models: Tao-MHD (red dotted lines) [*Tao et al.*, 2005] and SWMF-OH (blue dashed lines) [*Zieger et al.*, 2015]. The gray shaded regions mark the periods of the ground-based observations. As the Tao-MHD model is 1-D, the magnetic field magnitude plotted here is simply the absolute value of the modeled B_T. The magnetic field components refer to the radial-tangential-normal spacecraft coordinate system.

SWMF-OH (blue dashed lines)—all at a 1 h cadence. The gray columns identify the time periods of the ground-based H_3^+ observations.

Jupiter's average subsolar magnetopause distance is ~45–100 R_J (R_J is the equatorial radius, 71,492 km [*Khurana et al.*, 2004]) or (3.2–7.1) × 10^6 km. The mean difference in the Sun-Juno and Sun-Jupiter distances between 14 and 23 April was ~5 × 10^6 km, within the typical range for Jupiter's magnetopause distance. As seen from the Sun, the mean angle between Juno and Jupiter over this period was ~3°. Therefore, the solar wind structure measured by Juno would be impacting Jupiter's magnetopause at approximately the same time (to within an uncertainty of ±1.3 h, based on the mean radial solar wind velocity from Tao-MHD over this period, 423 km s^{-1}). An additional lag follows from the time scale for the propagation of a solar wind-driven event through Jupiter's magnetosphere prior to any auroral response, for which we estimate ~2–3 h, based on theoretical calculations of the time scales for magnetospheric compression and

magnetosphere-ionosphere coupling [*Cowley and Bunce*, 2003; *Cowley et al.*, 2007]. Thus, the total uncertainty between Juno's measurement of the solar wind and any corresponding variation in Jupiter's auroral emission is estimated to be roughly 0.7–4.3 h, relatively small given the other time scales involved. This uncertainty is smaller than the duration of the observations, indicated by the gray shaded regions in Figure 4, and so we have chosen not to apply any temporal offsets to any of the modeled or measured parameters plotted there.

The solar wind at Jupiter appears to have been relatively quiet over the period of this study. Magnetic field magnitudes on 14, 17, and 20 April, as measured by Juno, are all within 10% of each other. In contrast, by 23 April the magnetic field magnitude increased by a factor of ~2.6 over the 14-17-20 April mean value. The solar wind propagation models are generally consistent with each other and are able to reproduce much of the broad behavior of the magnetic field parameters measured by Juno throughout most of the period plotted in Figure 4, though they do not do as well at predicting small-scale IMF structure. Magnetic field components in this paper refer to the radial-tangential-normal coordinate system.

Based on Figure 4, there is little evidence for an auroral IR brightening driven by a pulse in solar wind dynamic pressure. There is some evidence for a solar wind shock arrival prior to the H_3^+ observations, however, meaning that Jupiter's magnetosphere may have been subjected to a period of compression and expansion. Such buffeting of the magnetosphere is expected to lead to main oval brightenings as well as enhancements in the ionospheric currents, heating the upper atmosphere [*Cowley et al.*, 2007; *Yates et al.*, 2014]. If Jupiter's magnetosphere was otherwise relatively quiescent between 14 and 24 April, a possibility supported at least by the solar wind parameters in Figure 4, then the effects of the previous compressions and expansions would diminish with each successive day and auroral temperatures would cool via a combination of IR radiation and atmospheric dynamics [*Melin et al.*, 2006; *Majeed et al.*, 2009; *Miller et al.*, 2010; *Yates et al.*, 2014]. The observed declining trend in mean H_3^+ temperature with time seen is consistent with such a gradual cooling; however, the variations in H_3^+ densities and radiances do not follow such a trend and require a different explanation.

Based on Figures 2 and 3, it is clear that the observed H_3^+ auroral emission patterns are driven primarily by H_3^+ column densities. The chemical lifetime of H_3^+ in Jupiter's ionosphere is relatively brief. For $T_e = 800$ K, the dissociative recombination rate of H_3^+ is ~3.06×10^{-8} cm^3 s^{-1} [*Kim and Fox*, 1994]. Using an auroral electron density of 10^5 cm^{-3} [*Grodent et al.*, 2001; *Lystrup et al.*, 2008], the estimated chemical lifetime of H_3^+ is ~326 s. Thermal time scales in the giant planets are much longer, on the order of days to months [*Achilleos et al.*, 1998; *Müller-Wodarg et al.*, 2006]. H_3^+ emissions should therefore track the incident particle precipitation patterns, modulated slightly by temperature, with a short temporal lag. As there is no obvious solar wind signature that would explain the observed 23 April auroral brightening, it is likely that internal magnetospheric processes are instead responsible.

4. Conclusion

High spectral resolution observations using Keck/NIRSPEC have enabled us to derive high-precision maps of H_3^+ temperatures, densities, and radiances across Jupiter's northern and southern auroral regions on 4 days in April 2016. Due to the spectral-mapping approach, short-term temporal variations are not detectable in this study. However, by comparing the mean properties across each region, we find evidence of significant variabilities in the H_3^+ aurorae over periods of several days. These variations primarily manifest as enhancements in emission intensity and column density, accompanied by reductions in temperature. Such signatures are consistent with increases in both the mean energy and energy flux of auroral particle precipitation.

Supporting evidence of the solar wind influence on Jupiter's H_3^+ aurora over the period of ground-based observations comes from measurements of the upstream IMF by the Juno spacecraft, along with solar wind propagation model results. A pulse of solar wind dynamic pressure appears to have driven a compression and expansion of Jupiter's magnetosphere in the days preceding the first ground-based observation on 14 April. Solar wind dynamic pressure and magnetic field over the rest of the period of study was quiescent and so would be expected to coincide with a gradual cooling of Jupiter's upper atmosphere. Ground-based observations of H_3^+ temperatures across three different regions of Jupiter's northern and southern aurorae do exhibit such a trend of decreasing temperature with time.

The strongest H_3^+ aurora from the four nights of ground-based observations, in terms of radiance and density, occurred on 23 April. Solar wind propagation models predict that this was a period of weak and constant dynamic pressure, and therefore it is unlikely that the observed brightening was caused by a shock-driven event. The 23 April auroral emissions must then be attributed to some other cause, with internal processes the most likely remaining source of auroral variability.

This study takes advantage of Juno IMF measurements in order to examine the impact of the solar wind on Jupiter's IR auroral emissions. Now that Juno has entered into its prime science orbits within Jupiter's magnetosphere, solar wind propagation models will serve as the primary means for predicting upstream solar wind conditions for future ground-based and space-based [e.g., *Adriani et al.*, 2014; *Gladstone et al.*, 2014] studies of Jupiter's auroral emissions. Combined with Juno particles and field measurements, additional information regarding the precipitating particle energies and fluxes, as well as the auroral currents, can be used to examine the energetics and dynamics of Jupiter's upper atmosphere in unprecedented detail.

Acknowledgments

The data presented herein were obtained at the W.M. Keck Observatory, which is operated as a scientific partnership among the California Institute of Technology, the University of California, and the National Aeronautics and Space Administration. The observatory was made possible by the generous financial support of the W. M. Keck Foundation. Funding for L.M. and J.O'D. comes from the National Aeronautics and Space Administration under grant NNX14AG72G, issued through the Planetary Astronomy Program. Additional support for J.O'D. comes from an appointment to the NASA Postdoctoral Program at Goddard Space Flight Center, administered by Universities Space Research Association under contract with NASA. Support for J. T.C. was from NASA grant STScI-GO14105.01A to Boston University. M.F. V. was supported by the National Science Foundation under award 1524651. H.M. and T.S. were supported by the UK STFC. The Juno MAG cruise data used in this study can be found on the Planetary Data System: https://ppi.pds.nasa.gov/search/view/?f=yes&id=pds://PPI/JNO-SS-3-FGM-CAL-V1.0. Keck data are publically accessible after 18 months (October 2017 for this data set, details here: https://koa.ipac.caltech.edu/UserGuide/access.html.

References

Achilleos, N., S. Miller, J. Tennyson, A. D. Aylward, I. Mueller-Wodarg, and D. Rees (1998), JIM: A time-dependent, three-dimensional model of Jupiter's thermosphere and ionosphere, *J. Geophys. Res.*, *103*, 20,089–20,112.

Adriani, A., et al. (2014), JIRAM, the Jovian Infrared Auroral Mapper, *Space Sci. Rev.*, doi:10.1007/s11214-014-0094-y.

Badman, S. V., et al. (2016), Weakening of Jupiter's main auroral emission during January 2014, *Geophys. Res. Lett.*, *43*, 988–997, doi:10.1002/2015GL067366.

Bagenal, F., et al. (2014), Magnetospheric science objectives of the Juno mission, *Space Sci. Rev.*, doi:10.1007/s11214-014-0036-8.

Baron, R. L., T. Owen, J. E. P. Connerney, T. Satoh, and J. Harrington (1996), Solar wind control of Jupiter's H3+ auroras, *Icarus*, *442*(120), 437–442.

Bolton, S. J., and the Juno Science Team (2010), The Juno mission, *Galileo's Medicean Moons their impact 400 years Discov.*, *269*(269), 92–100, doi:10.1017/S1743921310007313.

Bonfond, B., D. Grodent, J. C. Gérard, T. Stallard, J. T. Clarke, M. Yoneda, A. Radioti, and J. Gustin (2012), Auroral evidence of Io's control over the magnetosphere of Jupiter, *Geophys. Res. Lett.*, *39*, L01105, doi:10.1029/2011GL050253.

Chua, D., G. Parks, M. Brittnacher, W. Peria, G. Germany, J. Spann, and C. Carlson (2001), A comparison of substorms and pressure pulse related auroral activity, *J. Geophys. Res.*, *106*(A4), 5945–5956, doi:10.1029/2000JA003027.

Clarke, J. T., et al. (2009), Response of Jupiter's and Saturn's auroral activity to the solar wind, *J. Geophys. Res.*, *114*, A05210, doi:10.1029/2008JA013694.

Connerney, J. E. P., M. H. Acuña, N. F. Ness, and T. Satoh (1998), New models of Jupiter's magnetic field constrained by the Io flux tube footprint, *J. Geophys. Res.*, *103*(A6), 11,929–11,939.

Connerney, J. E. P., et al. (2017), The Juno magnetic field investigation, *Space Sci. Rev.*, doi:10.1007/s11214-017-0334-z.

Cowley, S. W. H., and E. J. Bunce (2003), Modulation of Jupiter's main auroral oval emissions by solar wind induced expansions and compressions of the magnetosphere, *Planet. Space Sci.*, *51*(1), 57–79, doi:10.1016/S0032-0633(02)00118-6.

Cowley, S. W. H., J. D. Nichols, and D. J. Andrews (2007), Modulation of Jupiter's plasma flow, polar currents, and auroral precipitation by solar wind-induced compressions and expansions of the magnetosphere: A simple theoretical model, *Ann. Geophys.*, *25*, 1433–1463.

Elphinstone, R. D., J. S. Murphree, and L. L. Cogger (1996), What is a global auroral substorm?, *Rev. Geophys.*, *34*(96), 169, doi:10.1029/96RG00483.

Galand, M., L. Moore, I. Mueller-Wodarg, M. Mendillo, and S. Miller (2011), Response of Saturn's auroral ionosphere to electron precipitation: Electron density, electron temperature, and electrical conductivity, *J. Geophys. Res.*, *116*, A09306, doi:10.1029/2010JA016412.

Gérard, J.-C., B. Bonfond, D. Grodent, A. Radioti, J. T. Clarke, G. R. Gladstone, J. H. Waite, D. Bisikalo, and V. I. Shematovich (2014), Mapping the electron energy in Jupiter's aurora: Hubble spectral observations, *J. Geophys. Res. Space Physics*, *119*, 9072–9088, doi:10.1002/2016JA022400.

Gladstone, G. R., et al. (2014), The ultraviolet spectrograph on NASA's Juno mission, *Space Sci. Rev.*, doi:10.1007/s11214-014-0040-z.

Grodent, D., J. H. Waite Jr., and J.-C. Gerard (2001), A self-consistent model of the Jovian auroral thermal structure, *J. Geophys. Res.*, *106*(A7), 12,933–12,952.

Hill, T. W. (2004), Auroral structures at Jupiter and Earth, *Adv. Sp. Res.*, *33*(11), 2021–2029, doi:10.1016/j.asr.2003.05.037.

Khurana, K. K., M. G. Kivelson, V. M. Vasyliūnas, N. Krupp, J. Woch, A. Lagg, B. H. Mauk, and W. S. Kurth (2004), The configuration of Jupiter's magnetosphere, in *Jupiter. The Planet, Satellites and Magnetosphere*, edited by F. Bagenal, T. E. Dowling, and W. B. McKinnon, pp. 593–616, Cambridge Univ. Press, Cambridge, U. K.

Kim, Y., and J. Fox (1994), The chemistry of hydrocarbon ions in the Jovian ionosphere, *Icarus*, *112*, 310–324.

Kimura, T., et al. (2015), Transient internally driven aurora at Jupiter discovered by Hisaki and the Hubble Space Telescope, *Geophys. Res. Lett.*, *42*, 1–7, doi:10.1002/2015GL063354.

Kita, H., et al. (2016), Characteristics of solar wind control on Jovian UV auroral activity deciphered by long-term Hisaki EXCEED observations: Evidence of preconditioning of the magnetosphere?, *Geophys. Res. Lett.*, *43*, 6790–6798, doi:10.1002/2016GL069481.

Lystrup, M. B., S. Miller, N. Dello Russo, J. R. J. Vervack, and T. Stallard (2008), First vertical ion density profile in Jupiter's auroral atmosphere: Direct observations using the Keck II telescope, *Astrophys. J.*, *677*(1), 790–797, doi:10.1086/529509.

Majeed, T., J. H. Waite, S. W. Bougher, and G. R. Gladstone (2009), Processes of auroral thermal structure at Jupiter: Analysis of multispectral temperature observations with the Jupiter thermosphere general circulation model, *J. Geophys. Res.*, *114*, E07005, doi:10.1029/2008JE003194.

Mclean, I. S., et al. (1998), The design and development of NIRSPEC: A near-infrared Echelle spectrograph for the Keck II telescope, *Proc. SPIE 3354, Infrared Astron. Instrum.*, *566*(March), 566–578, doi:10.1117/12.317283.

Melin, H., S. Miller, T. Stallard, and D. Grodent (2005), Non-LTE effects on H_3^+ emission in the Jovian upper atmosphere, *Icarus*, *178*(1), 97–103, doi:10.1016/j.icarus.2005.04.016.

Melin, H., S. Miller, T. Stallard, C. Smith, and D. Grodent (2006), Estimated energy balance in the Jovian upper atmosphere during an auroral heating event, *Icarus*, *181*(1), 256–265, doi:10.1016/j.icarus.2005.11.004.

Melin, H., T. S. Stallard, J. O'Donoghue, S. V. Badman, S. Miller, and J. S. D. Blake (2014), On the anticorrelation between H_3^+ temperature and density in giant planet ionospheres, *Mon. Not. R. Astron. Soc.*, *438*(2), 1611–1617, doi:10.1093/mnras/stt2299.

Miller, S., et al. (2000), The role of H_3^+ in planetary atmospheres, *Philos. Trans. R. Soc. A Math. Phys. Eng. Sci.*, *358*, 2485–2502.

Miller, S., T. Stallard, H. Melin, and J. Tennyson (2010), H_3^+ cooling in planetary atmospheres, *Faraday Discuss.*, *147*, 283, doi:10.1039/c004152c.

Millward, G., S. Miller, T. Stallard, and A. Aylward (2002), On the dynamics of the Jovian ionosphere and thermosphere III. The modelling of auroral conductivity, *Icarus*, *160*(1), 95–107, doi:10.1006/icar.2002.6951.

Müller-Wodarg, I. C. F., M. Mendillo, R. Yelle, and A. Aylward (2006), A global circulation model of Saturn's thermosphere, *Icarus*, *180*(1), 147–160, doi:10.1016/j.icarus.2005.09.002.

Müller-Wodarg, I. C. F., L. Moore, M. Galand, S. Miller, and M. Mendillo (2012), Magnetosphere-atmosphere coupling at Saturn: 1—Response of thermosphere and ionosphere to steady state polar forcing, *Icarus*, *221*(2), 481–494, doi:10.1016/j.icarus.2012.08.034.

Neale, L., S. Miller, and J. Tennyson (1996), Spectroscopic properties of the H3+ molecule: A new calculated line list, *Astrophys. J.*, *464*, 516–520.

Nichols, J. D., E. J. Bunce, J. T. Clarke, S. W. H. Cowley, J.-C. Gérard, D. Grodent, and W. R. Pryor (2007), Response of Jupiter's UV auroras to interplanetary conditions as observed by the Hubble Space Telescope during the Cassini flyby campaign, *J. Geophys. Res.*, *112*, A02203, doi:10.1029/2006JA012005.

Nichols, J. D., J. T. Clarke, J. C. Gérard, D. Grodent, and K. C. Hansen (2009), Variation of different components of Jupiter's auroral emission, *J. Geophys. Res.*, *114*, A06210, doi:10.1029/2009JA014051.

O'Donoghue, J., H. Melin, T. S. Stallard, G. Provan, L. Moore, S. V. Badman, S. W. H. Cowley, K. H. Baines, S. Miller, and J. S. D. Blake (2016), Ground-based observations of Saturn's auroral ionosphere over three days: Trends in H_3^+ temperature, density and emission with Saturn local time and planetary period oscillation, *Icarus*, *263*, 44–55, doi:10.1016/j.icarus.2015.04.018.

Opher, M., E. C. Stone, and P. Liewer (2006), The effects of a local interstellar magnetic field on Voyager 1 and 2 observations, *Astrophys. J.*, *640*, 71–74.

Opher, M., F. A. Bibi, G. Toth, J. D. Richardson, V. V. Izmodenov, and T. I. Gombosi (2009), A strong, highly-tilted interstellar magnetic field near the solar system, *Nature*, *462*(7276), 1036–1038, doi:10.1038/nature08567.

Seiff, A. (1997), Thermal structure of Jupiter's upper atmosphere derived from the Galileo Probe, *Science*, *276*(5309), 102–104, doi:10.1126/science.276.5309.102.

Smith, C. G. A., and A. D. Aylward (2009), Coupled rotational dynamics of Jupiter's thermosphere and magnetosphere, *Ann. Geophys.*, *27*, 199–230.

Stallard, T., S. Miller, G. Millward, and R. D. Joseph (2002), On the dynamics of the Jovian ionosphere and thermosphere II. The measurement of H3+ vibrational temperature, column density, and total emission, *Icarus*, *156*(2), 498–514, doi:10.1006/icar.2001.6793.

Tao, C., R. Kataoka, H. Fukunishi, Y. Takahashi, and T. Yokoyama (2005), Magnetic field variations in the Jovian magnetotail induced by solar wind dynamic pressure enhancements, *J. Geophys. Res.*, *110*, A11208, doi:10.1029/2004JA010959.

Tao, C., S. V. Badman, and M. Fujimoto (2011), UV and IR auroral emission model for the outer planets: Jupiter and Saturn comparison, *Icarus*, *213*(2), 581–592, doi:10.1016/j.icarus.2011.04.001.

Thomas, N., F. Bagenal, T. Hill, and J. Wilson (2004), The Io neutral clouds and plasma torus, in *Jupiter: The Planet, Satellites and Magnetosphere*, edited by F. Bagenal, T. E. Dowling, and W. B. McKinnon, pp. 561–591, Cambridge Univ. Press, Cambridge.

Tóth, G., et al. (2012), Adaptive numerical algorithms in space weather modeling, *J. Comput. Phys.*, *231*(3), 870–903, doi:10.1016/j.jcp.2011.02.006.

Yates, J. N., N. Achilleos, and P. Guio (2014), Response of the Jovian thermosphere to a transient "pulse" in solar wind pressure, *Planet. Space Sci.*, *91*, 27–44, doi:10.1016/j.pss.2013.11.009.

Zieger, B., G. Tóth, M. Opher, and T. Gombosi (2015), Solar wind prediction at Pluto during the new horizons flyby: Results from a two-dimensional multifluid MHD model of the outer heliosphere, Abstract SM31D-2539 presented at 2015 Fall Meeting, pp. 1–2, AGU, San Francisco, Calif.